ARTICLES

Journal of Semiconductors
(2020) 41, 052201
doi: 10.1088/1674-4926/41/5/052201

Comprehensive first-principles studies on phase stability of copper-based halide perovskite derivatives $A_lCu_mX_n$ (A = Rb and Cs; X = Cl, Br, and I)

Zhongti Sun[1, 2], Xiwen Chen[1, 2], and Wanjian Yin[1, 2, 3, †]

[1]College of Energy, Soochow Institute for Energy and Materials InnovationS (SIEMIS), Soochow University, Suzhou 215006, China

[2]Jiangsu Provincial Key Laboratory for Advanced Carbon Materials and Wearable Energy Technologies, Soochow University, Suzhou 215006, China

[3]Key Lab of Advanced Optical Manufacturing Technologies of Jiangsu Province & Key Lab of Modern Optical Technologies of Education Ministry of China, Soochow University, Suzhou 215006, China

Abstract: Recently, inorganic copper-based halide perovskites and their derivatives (CHPs) with chemical formulas $A_lCu_mX_n$ (A = Rb and Cs; X = Cl, Br and I; *l*, *m*, and *n* are integers.), have received increasing attention in the photoluminescence field, due to their lead-free, cost-effective, earth-abundant and low electronic dimensionality. Ascribed to flexible valence charge of Cu (Cu^{1+} and Cu^{2+}) and complex competing phases, the crystal structures and phase stabilities of CHPs are complicated and ambiguous, which limits their experimental applications. Via comprehensive first-principles calculations, we have investigated thermodynamic stabilities of possible crystal phases for $A_lCu_mX_n$ by considering all the possible secondary phases existing in inorganic crystal structure database (ICSD). Our results are in agreement with existing experiments and further predicted the existence of 10 stable CHPs, i.e. $Rb_3Cu_2Br_5$, $Rb_3Cu_2I_5$, $RbCu_2Cl_3$, Rb_2CuI_3, Rb_2CuBr_4, $RbCuBr_3$, $Rb_3Cu_2Br_7$, $Cs_3Cu_2Br_7$, $Cs_3Cu_2Cl_7$ and $Cs_4Cu_5Cl_9$, which have not yet been reported in experiments. This work provides a phase and compositional map that may guide experiments to synthesize more novel inorganic CHPs with diverse properties for potential functional applications.

Key words: first-principles calculations; copper-based halide perovskite; stability; phase diagram

Citation: Z T Sun, X W Chen, and W J Yin, Comprehensive first-principles studies on phase stability of copper-based halide perovskite derivatives $A_lCu_mX_n$ (A = Rb and Cs; X = Cl, Br, and I)[J]. *J. Semicond.*, 2020, 41(5), 052201. http://doi.org/10.1088/1674-4926/41/5/052201

1. Introduction

Artificial lighting accounts for one-fifth of global electricity consumption, with a half of that amount consumed by inefficient incandescent and fluorescent emission sources[1, 2]. Recently, metal halide perovskites have gained much attention thanks to their outstanding optoelectronic characters including high photo-absorption efficiency, tunable emission across the entire visible spectrum, exceptional defect tolerance and low-cost synthesis processing[3–5]. Nevertheless, so far, the best-performing halides contain hazardous and bioaccumulative lead and have unsatisfactory stability against moisture and temperature, particularly for organic–inorganic hybrid lead halide perovskites[6–9]. Nowadays replacing the toxic Pb in the perovskite structures with alternative non-toxic, environment-friendly, earth-abundant and cost-effective elements such as transition metals is of critical importance for improving light-emitting capability[10–14].

Recently, Cu-based halide perovskites and their derivatives (CHPs) have been emerging and attracted increasing attention because of the replacement of Pb with abundant, economic and environment-friendly Cu element[10–14]. The rich chemistry of Cu with multiple valence states and low coordination number lead to their complex crystal structures, including 2D layer, 1D chain, 0D isolated units[15]. These low-dimensional crystal structures, resulting in low electronic dimensionality, may give rise to large exciton binding energy (E_b) and high photoluminescent quantum yield (PLQY) due to the quantum confinement effect (QCE)[14, 16]. For example, E_b of 0D Cs_4PbBr_6 with ~240 meV is much larger than 3D $CsPbBr_3$ with ~18 meV[8, 9]. Recently, Hosono *et al.* reported in experiment that $Cs_3Cu_2I_5$ (named as 325-type) films and single crystals owned high PLQY with ~60% and ~90%, respectively[14]. In crystal structure of $Cs_3Cu_2I_5$ compounds, spatially isolated $[Cu_2I_5]^{3-}$ anion is surrounded by Cs^+ cations and two Cu^+ ions possess lower coordination with a tetrahedral and a trigonal types, respectively. Spatially isolated [Cu–I] polyhedron induces enormous E_b with ~490 meV, much higher than Pb-based halide perovskites[14]. Zhao *et al.* also discovered that another type of CHP Cs_2CuX_4 (X = Cl, Br, and Br/I, named as 214-type) quantum dots possessed high PLQY of ~50% for blue-green light emitting and excellent air and photo-stability, where spatially isolated [Cu–X] tetrahedron is also surrounded by Cs^+ ions and Cu^{2+} ion possessing tetrahedral coordinations[17]. In the Cs_2CuBr_4 synthesis processing, the phenomenon about Cu^{2+} ion partially reducing to Cu^+ was observed through X-ray diffraction and the X-ray photoelectron spectroscopy characteristics[17].

Apart from 325- and 214-type CHPs which have been reported in lighting application, other phases such as 123-,

Correspondence to: W J Yin, wjyin@suda.edu.cn
Received 21 FEBRUARY 2020; Revised 3 MARCH 2020.

Table 1. The Space group of existing CHPs with various types encompassing 325-, 123-, 213-, 459-, 214-, 113-, and 327-type from inorganic crystal structure database (ICSD). '√' and blank grid symbol indicates the existing and non-existing phase in experiment, respectively.

Type	Space group (No.)	Rb			Cs		
		Cl	Br	I	Cl	Br	I
325	Pnma (62)				√	√	√
123	Cmcm (63)		√	√	√	√	√
213	Pnma (62)	√	√				
459	Pc (7)	√					
214	Pnma (62)				√	√	
	Cmca (64)	√					
	P6122 (178)				√		
113	C2221 (20)					√	
	Pbcn (60)	√					
327	Ccca (68)	√					

113-, 213-, 327-, and 459-type, have also been reported in experiments[15, 18–21]. Diverse phases of CHPs with isolated [Cu–X] building blocks provide a treasure trove for potential applications in lighting. Nevertheless, the phase stability of $A_lCu_mX_n$ (A = Rb and Cs; X = Cl, Br, and I) have not been clearly investigated as shown in Table 1. This has hampered further development of those materials for practical applications. Meanwhile, the ample crystal structures together with variable valence states of Cu, make it difficult to control the synthesis of CHPs. Therefore, it is necessary to provide a landscape of phase stability for CHPs and suggestions of chemical environments to synthesize particular compounds per request.

In this paper, first-principles calculations are performed to comprehensively investigate the thermodynamic stability of CHPs ($A_lCu_mX_n$, A = Rb and Cs; X = Cl, Br, and I) based on thermodynamic equilibrium growth condition. In total, there are 42 CHPs compounds with seven kinds of stoichiometric ratio including $A_3Cu_2X_5$, ACu_2X_3, A_2CuX_3, $A_4Cu_5X_9$, A_2CuX_4, $ACuX_3$, and $A_3Cu_2X_7$, as shown in Table 1. For chemical environments and stability calculations, all possible competing phases including compositional elements Rb, Cs, Cu, Cl, Br, I, binary compounds and ternary compounds from inorganic crystal structure database (ICSD) have been considered. We have found that most of existing $A_lCu_mX_n$ phases in experiments have a stable growth region and positive decomposition energy in our calculations, which confirms the reliability of our calculations. Moreover, we also acquire ten new and stable phases encompassing $Rb_3Cu_2I_5$, $Rb_3Cu_2Br_5$, $RbCu_2Cl_3$, Rb_2CuI_3, Rb_2CuBr_4, $RbCuBr_3$, $Rb_3Cu_2Br_7$, $Cs_3Cu_2Br_7$, $Cs_3Cu_2Cl_7$, and $Cs_4Cu_5Cl_9$, which are not yet reported experimentally. Therefore, our work provides prospective guidance for experiment to synthesize the above phases, amplifying the scope of phases of CHPs.

2. Computational details

All of the calculations were executed with spin-unrestricted density functional theory method, as implemented in the Vienna ab-initio simulation package (VASP)[22] by using the projector augmented wave (PAW) pseudopotential[23]. We employ the generalized gradient approximation (GGA) parametrized by Perdew, Burker, and Ernzerhof (PBE)[24] as electronic exchange-correlation functional. The kinetic energy cutoff with plane wave basis set is 400 eV and the *k*-point meshes with grid spacing of $2\pi \times 0.025$ Å^{-1}. All of the structures were fully relaxed until the total energy and force per atom were less than 10^{-4} eV and –0.01 eV/Å, respectively.

To evaluate the thermodynamic stability of CHPs $A_lCu_mX_n$ (A = Rb and Cs; X = Cl, Br, and I) with different types, we first calculate the chemical potential range for equilibrium growth of compound to identify the proper chemical potentials for synthesizing particular compounds in experiments[25, 26]. Second, we quantitatively calculated the thermodynamic stability via considering the optimal decomposition pathways to their competing phases through linear programming. For calculation of chemical potential range, the chemical potential μ_α (α is the element that constituted to the CHPs) is constrained by the values that keep a stable host compound, and avoid the formation of other competing phases, including elemental solids. The thermodynamic equilibrium growth conditions need to satisfy the following three relations.

$$l\mu_A + m\mu_{Cu} + n\mu_X = \Delta H(A_lCu_mX_n), \quad l, m, n = 1, 2, \ldots, N, \tag{1}$$

$$\mu_\alpha \leqslant 0, \quad \alpha = A, Cu, X, \tag{2}$$

$$h_i\mu_A + k_i\mu_{Cu} + l_i\mu_X \leqslant \Delta H(A_{h_i}Cu_{k_i}X_{l_i}), \quad i = 1, 2, \ldots, N, \tag{3}$$

where μ_α is the chemical potential of constituent element α referring to the stable solid/gas in the growth conditions. ΔH is the formation enthalpy, $A_lCu_mX_n$ and $A_{h_i}Cu_{k_i}X_{l_i}$ represent the thermodynamic equilibrium phase and all the existing competing phases, respectively. Eq. (1) is for the thermodynamic equilibrium growth condition, Eq. (2) is to avoid the atomic species that depositing to elemental phases, Eq. (3) is to hamper all the existing competing phase.

Then, the thermodynamic stability of CHPs $A_lCu_mX_n$ was furtherly confirmed through decomposition energy calculation based on optimal decomposition pathway (ODP) using linear programming method. Specific details are as follows:

$$A_lCu_mX_n \rightarrow \sum_{i=1}^{i} x_iA_{h_i}Cu_{k_i}X_{l_i}, \tag{4}$$

$$\Delta H_d = \sum_{i=1}^{i} x_iE(A_{h_i}Cu_{k_i}X_{l_i}) - E(A_lCu_mX_n), \tag{5}$$

$$\sum_{i=1}^{i} x_ih_i = l, \quad \sum_{i=1}^{i} x_ik_i = m, \quad \sum_{i=1}^{i} x_il_i = n, \tag{6}$$

$$0 \leqslant x_i \leqslant \min\left(\frac{l}{h_i}, \frac{m}{k_i}, \frac{n}{l_i}\right), \tag{7}$$

where the x_i is the molar fraction of possible competing phases, unknown variables. Eq. (4) is the decomposition pathway of host compounds, Eq. (5) is the decomposition energy between existing competing phases and host phase, Eq. (6) is

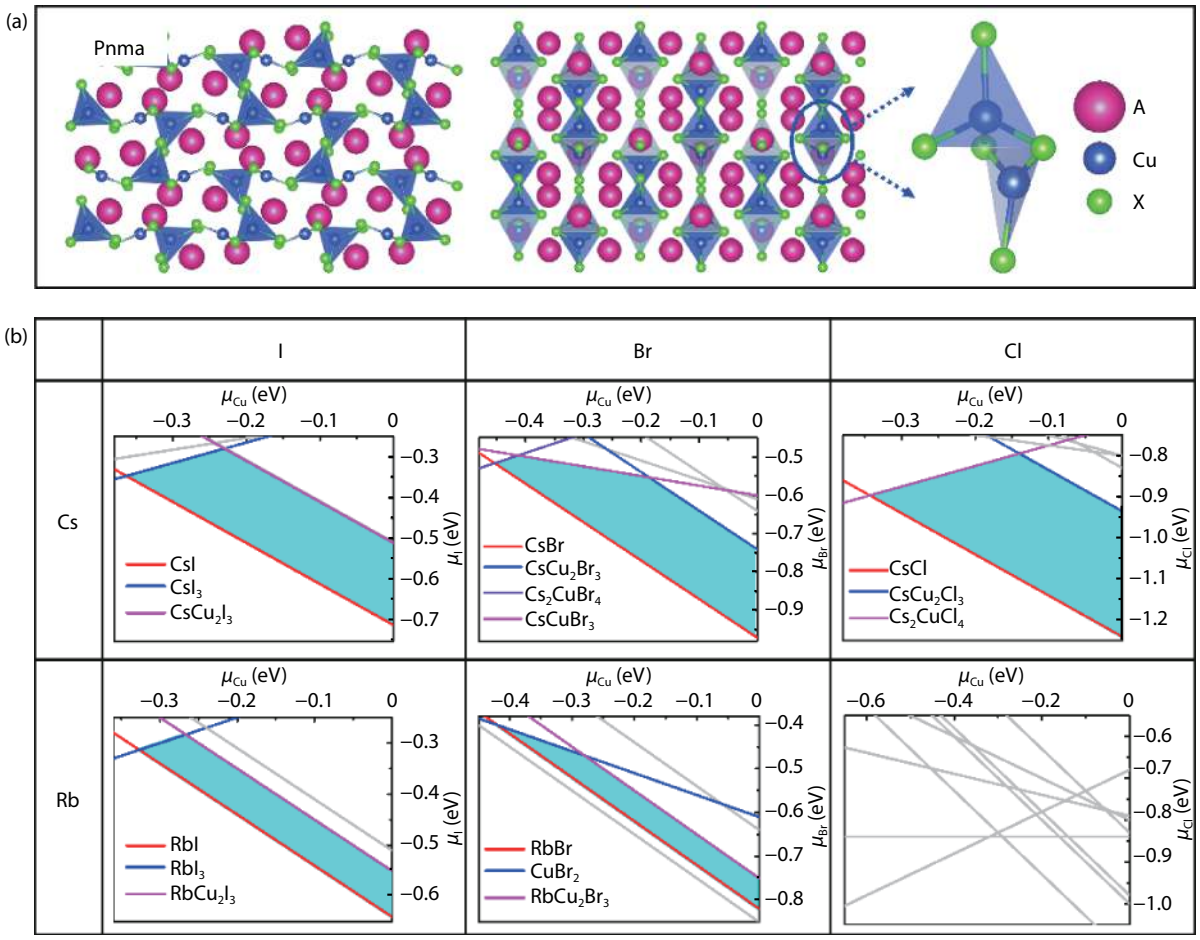

Fig. 1. (Color online) (a) The optimized structure of CHPs with 325-type, they own the isostructural model with space group of Pnma, isolated $[Cu_2X_5]^{3-}$ anion unit is composed of two types of Cu^+ sites, a trigonal site and a tetragonal site. (b) Calculated phase stability regions versus μ_{Cu} and μ_X (referring to the chemical potential of Cu and X from that of their elementary substance) from left to right for the X site of I, Br, and Cl element and up to down for Cs and Rb element on A site, respectively. The cyan polygon region represents thermodynamic stability growth region, which is encircled by possible competing phases using colored line (red, blue, violet, and pink). A, Cu, and X atoms are in purple, coral and brown, respectively.

the mass-conservation constraints for all atomic species, Eq. (7) is the minimum value of x_i. The linear programming approach ensures that the calculated decomposition energy is based on the optimal decomposition pathway. If the value of ΔH_d is a positive number, then this decomposition reaction is an endothermic reaction, indicating that this compound is thermodynamically stable.

3. Results and discussions

3.1. $A_3Cu_2X_5$ phase

$A_3Cu_2X_5$ phase exhibits orthorhombic crystal structure with space group of Pnma (No. 62) as shown in Fig. 1(a). It has two types of Cu^+ ion sites, a tetrahedral site and a trigonal site, each of which constitutes spatially isolated $[Cu_2X_5]^{3-}$ (X = Cl, Br, I), encircled by A^+ (A = Rb, Cs) ions. Thermodynamic stability of six kinds of 325-type CHPs are evaluated based on thermodynamic equilibrium growth conditions and decomposition energy with ODP as shown in Fig. 1(b) and Table 2, respectively. Except for $Rb_3Cu_2Cl_5$, all five compounds possess stability region in cyan polygon. In consistent with experiments, $Cs_3Cu_2X_5$ (X = Cl, Br, I) have been synthesized in experiments and $Cs_3Cu_2I_5$ has been applied to the luminescent equipment with high PLQY[14]. Our results show that $Rb_3Cu_2I_5$ and $Rb_3Cu_2Br_5$ can also be stable but $Rb_3Cu_2Cl_5$ is unstable. The minimum decomposition energies together with corresponding decomposition pathways calculated by linear programing method have been shown in Table 2. Interestingly, the ODP of $Cs_3Cu_2Cl_5$ perovskite are different for $Cs_3Cu_2Br_5$ and $Cs_3Cu_2I_5$, i.e. $Cs_3Cu_2X_5 \rightarrow 2CsX + CsCu_2X_3$, X = Br and I, their ΔH_d are 25 and 29 meV/atom for the X site of Br and I, respectively. These decomposition reactions are non-redox processes. In contrast to these two compounds, the ODP of $Cs_3Cu_2Cl_5$ perovskite is a disproportionation reaction with ΔH_d of 33 meV/atom, namely $Cs_3Cu_2Cl_5 \rightarrow Cu + CsCl + Cs_2CuCl_4$, the competing phase has CsCl secondary phase, it is also consistent with experiment that CsCl additional phase observed as minor impurity[15]. So it should be carefully controlled in the synthesis process. If the decomposition pathway of $Cs_3Cu_2Cl_5$ perovskite is same as the ODP of $Cs_3Cu_2X_5$ (X = Br and I), then its decomposition energy is 39 meV/atom, which is a little larger than the ODP by 6 meV/atom. For $Rb_3Cu_2X_5$ (X = Cl, Br, and I), their ODPs are all non-redox reactions, $Rb_3Cu_2I_5$ phase owns the similar ODP with the $Cs_3Cu_2I_5$ phase by ΔH_d of 12 meV/atom, but different from the ODP of $Rb_3Cu_2Br_5$ phase with ΔH_d of 5 meV/atom, i.e.,

Table 2. Calculated decomposition energies together with ODP in the CHPs $A_lCu_mX_n$ (A = Rb and Cs; X = Cl, Br, and I; *l*, *m*, and *n* are integers).

Compound		ΔH_d (meV/atom)	Optimal decomposition pathway
325-type	$Cs_3Cu_2I_5$	25	$Cs_3Cu_2I_5 \rightarrow 2CsI + CsCu_2I_3$
	$Cs_3Cu_2Br_5$	29	$Cs_3Cu_2Br_5 \rightarrow 2CsBr + CsCu_2Br_3$
	$Cs_3Cu_2Cl_5$	33	$Cs_3Cu_2Cl_5 \rightarrow Cu + CsCl + Cs_2CuCl_4$
	$Rb_3Cu_2I_5$	13	$Rb_3Cu_2I_5 \rightarrow 2RbI + RbCu_2I_3$
	$Rb_3Cu_2Br_5$	5	$Rb_3Cu_2Br_5 \rightarrow 4/3Rb_2CuBr_3 + 1/3RbCu_2Br_3$
	$Rb_3Cu_2Cl_5$	–2	$Rb_3Cu_2Cl_5 \rightarrow 7/5RbCl + 2/5Rb_4Cu_5Cl_9$
123-type	$CsCu_2I_3$	0	$CsCu_2I_3 \rightarrow 4/3CuI + 1/3Cs_3Cu_2I_5$
	$CsCu_2Br_3$	22	$CsCu2Br_3 \rightarrow 4/3CuBr + 1/3Cs_3Cu_2Br_5$
	$CsCu_2Cl_3$	24	$CsCu_2Cl_3 \rightarrow 4/3CuCl + 1/3Cu_3Cu_2Cl_5$
	$RbCu_2I_3$	23	$RbCu_2I_3 \rightarrow RbI + 2CuI$
	$RbCu_2Br_3$	28	$RbCu_2Br_3 \rightarrow 3/2CuBr + 1/2Rb_2CuBr_3$
	$RbCu_2Cl_3$	6	$RbCu_2Cl_3 \rightarrow 3/4CuCl + 1/4Rb_4Cu_5Cl_9$
213-type	Cs_2CuI_3	–22	$Cs_2CuI_3 \rightarrow 1/2CsI + 1/2Cs_3Cu_2I_5$
	Cs_2CuBr_3	–16	$Cs_2CuBr_3 \rightarrow 1/2CsBr + 1/2Cs_3Cu_2Br_5$
	Cs_2CuCl_3	–19	$Cs_2CuCl_3 \rightarrow 1/2CsCl + 1/2Cs_3Cu_2Cl_5$
	Rb_2CuI_3	6	$Rb_2CuI_3 \rightarrow 3/2RbI + 1/2RbCu_2I_3$
	Rb_2CuBr_3	6	$Rb_2CuBr_3 \rightarrow 3/2RbBr + 1/2RbCu_2Br_3$
	Rb_2CuCl_3	8	$Rb_2CuCl_3 \rightarrow 1/2Cu + RbCl + 1/2Rb_2CuCl_4$
459-type	$Cs_4Cu_5I_9$	–20	$Cs_4Cu_5I_9 \rightarrow 3/4Cs_3Cu_2I_5 + 7/4CsCu_2I_3$
	$Cs_4Cu_5Br_9$	–9	$Cs_4Cu_5Br_9 \rightarrow 3/4Cs_3Cu_2Br_5 + 7/4CsCu_2Br_3$
	$Cs_4Cu_5Cl_9$	8	$Cs_4Cu_5Cl_9 \rightarrow 3/4Cs_3Cu_2Cl_5 + 7/4CsCu_2Cl_3$
	$Rb_4Cu_5I_9$	–17	$Rb_4Cu_5I_9 \rightarrow 3/2RbI + 5/2RbCu_2I_3$
	$Rb_4Cu_5Br_9$	–4	$Rb_4Cu_5Br_9 \rightarrow Rb_2CuBr_3 + 2RbCu_2Br_3$
	$Rb_4Cu_5Cl_9$	22	$Rb_4Cu_5Cl_9 \rightarrow 12/5Cu + 1/5Rb_2CuCl_3 + 6/5Rb_3Cu_2Cl_7$
214-type	Cs_2CuI_4	–17	$Cs_2CuI_4 \rightarrow 1/2CsI_3 + 1/2Cs_3Cu_2I_5$
	Cs_2CuBr_4	14	$Cs_2CuBr_4 \rightarrow 1/2CsBr + 1/4CsBr_3 + 1/2CsCuBr_3 + 1/4Cs_3Cu_2Br_5$
	Cs_2CuCl_4	34	$Cs_2CuCl_4 \rightarrow CsCl + CsCuCl_3$
	Rb_2CuI_4	–2	$Rb_2CuI_4 \rightarrow RbI + 1/2RbI_3 + 1/2RbCu_2I_3$
	Rb_2CuBr_4	10	$Rb_2CuBr_4 \rightarrow 2RbBr + CuBr_2$
	Rb_2CuCl_4	–9	$Rb_2CuCl_4 \rightarrow 1/2RbCl + 1/2Rb_3Cu_2Cl_7$
113-type	$CsCuI_3$	–34	$CsCuI_3 \rightarrow 1/2CsI_3 + 1/2CsCu_2I_3$
	$CsCuBr_3$	19	$CsCuBr_3 \rightarrow 1/2CuBr_2 + 1/2Cs_2CuBr_4$
	$CsCuCl_3$	5	$CsCuCl_3 \rightarrow 1/2CuCl_2 + 1/2Cs_2CuCl_4$
	$RbCuI_3$	–42	$RbCuI_3 \rightarrow 1/2RbI_3 + 1/2RbCu_2I_3$
	$RbCuBr_3$	21	$RbCuBr_3 \rightarrow RbBr + CuBr_2$
	$RbCuCl_3$	–10	$RbCuCl_3 \rightarrow 1/3CuCl_2 + 1/3Rb_3Cu_2Cl_7$
327-type	$Cs_3Cu_2I_7$	–31	$Cs_3Cu_2I_7 \rightarrow CsI_3 + 1/2Cs_3Cu_2I_5 + 1/2CsCu_2I_3$
	$Cs_3Cu_2Br_7$	9	$Cs_3Cu_2Br_7 \rightarrow Cs_2CuBr_4 + CsCuBr_3$
	$Cs_3Cu_2Cl_7$	9	$Cs_3Cu_2Cl_7 \rightarrow CsCuCl_3 + Cs_2CuCl_4$
	$Rb_3Cu_2I_7$	–31	$Rb_3Cu_2I_7 \rightarrow RbI + RbI_3 + RbCu_2I_3$
	$Rb_3Cu_2Br_7$	23	$Rb_3Cu_2Br_7 \rightarrow 3RbBr + 2CuBr_2$
	$Rb_3Cu_2Cl_7$	15	$Rb_3Cu_2Cl_7 \rightarrow Rb_2CuCl_4 + RbCuCl_3$

$Rb_3Cu_2Br_5 \rightarrow 4/3Rb_2CuBr_3 + 1/3RbCu_2Br_3$. For $Rb_3Cu_2Cl_5$, because of more complex competing phases, the ODP with ΔH_d of –2 meV/atom is $Rb_3Cu_2Cl_5 \rightarrow 7/5RbCl + 2/5Rb_4Cu_5Cl_9$, suggesting its poorer stability than its bromide and iodide counterparts.

3.2. ACu_2X_3 phase

ACu_2X_3 phase exhibits orthorhombic space group of Cmcm (No. 63), the 1D chain with two [Cu–X] tetrahedra through edge-sharing in a row, isolated by A^+ ion, as shown in Fig. 2(a). Fig. 2(b) shows the stability region of ACu_2X_3 phase in chemical potential map. The results show that all the ACu_2X_3 (A = Rb and Cs; X = Cl, Br, and I) compounds have thermodynamic stability region with cyan polyhedron, surrounded by the boundary composed of competing phases, which is in agreement with existing experiments that five of them have been synthesized successfully in experiments[15], except for $RbCu_2Cl_3$. The minimum decomposition energies together with corresponding decomposition pathways have been shown in Table 2, well matching the thermodynamic stability region calculations. $CsCu_2X_3$ possess the same ODP, i.e., $CsCu_2X_3 \rightarrow 4/3CuX + 1/3Cs_3Cu_2X_5$ (X = Cl, Br, and I). Their corresponding ΔH_d are 0, 22, and 24 meV/atom for $CsCu_2I_3$, $CsCu_2Br_3$, $CsCu_2Cl_3$, respectively. The ODPs of $RbCu_2I_3$, $RbCu_2Br_3$, and $RbCu_2Cl_3$ are all different, i.e., $RbCu_2I_3 \rightarrow RbI + 2CuI$, $RbCu_2Br_3 \rightarrow 3/2CuBr + 1/2Rb_2CuBr_3$, $RbCu_2Cl_3 \rightarrow 3/4CuCl + 1/4Rb_4Cu_5Cl_9$. Their decomposition energies are 23, 27, and 6 meV/atom for $RbCu_2I_3$, $RbCu_2Br_3$, and $RbCu_2Cl_3$, respectively. Considering that $CsCu_2I_3$ has a small stability region and tiny ΔH_d, experimental synthesis of its Rb counterpart may be

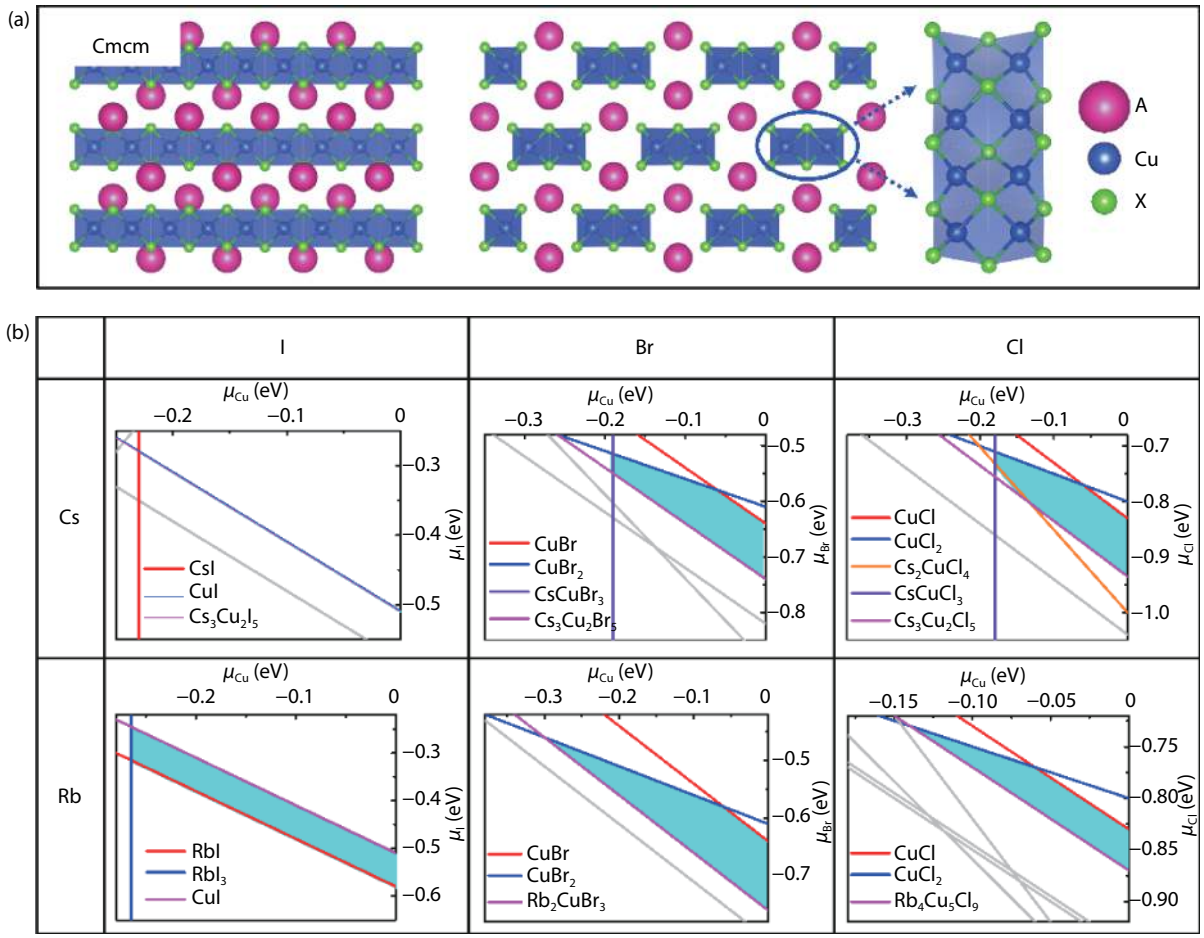

Fig. 2. (Color online) (a) The structure model of CHPs with 123-type, they all own octahedral structure with the space group of Cmcm (No. 63), composed of edge-sharing [CuX_4] tetrahedron 1D chain. (b) Calculated thermodynamic stability regions of ACu_2X_3 (A = Rb and Cs; X = Cl, Br, and I) CHPs versus μ_{Cu} and μ_X (deviation of actual chemical potential of Cu and X from that of their elementary substance). The above from left to right is the CHP for the X site of I, Br, and Cl element, and up to down is for Cs and Rb element on A site, respectively. The cyan polygon region represents thermodynamic stable interval, which is surrounded by competing phases using colored line (red, blue, orange, violet, and pink). A, Cu, and X atoms are in purple, coral and brown, respectively.

easier since $RbCu_2Cl_3$, has much larger stable region and corresponding larger decomposition energies, which may be more useful in photoluminescence fields than $CsCu_2X_3$.

3.3. $A_2Cu_1X_3$ phase

In contrast from the ACu_2X_3 phase with wider 1D chain by two Cu^+ ions in one row, the A_2CuX_3 phase with the symmetry of Pnma (No. 62) also owns a 1D chain with only one Cu^+ ion via vertex-sharing one line in Fig. 3(a). Their phase stability regions versus the chemical potential of Cu and X element are shown in Fig. 3(b). Only Rb_2CuI_3 and Rb_2CuBr_3 possess slim stability region with cyan polyhedron. Meanwhile, Rb_2CuBr_3 phase has been synthesized successfully in experiments[15]. Even though Rb_2CuCl_3 perovskite has no stability region from simulation, the decomposition energy calculations confirmed that its ΔH_d with ODP is a positive number with 8 meV/atom, namely $Rb_2CuCl_3 \rightarrow 1/2Cu + RbCl + 1/2Rb_2CuCl_4$, as shown in Table 2. Indeed, Rb_2CuCl_3 exists in experiments and the additional competing phase RbCl was also observed, consistent with our predictions in the ODP[15]. In addition, $Rb_2CuI(Br)_3$ phases own the same ODP with positive ΔH_d, i.e. $Rb_2CuX_3 \rightarrow 3/2RbX + 1/2RbCu_2X_3$, X = Br, I. While the 213-type CHP with the A site of Cs element also possess the same ODP, namely $Cs_2CuX_3 \rightarrow 1/2CsX + 1/2Cs_3Cu_2X_5$, X = Cl, Br, and I, their ΔH_d are all negative indicating their instability.

3.4. $A_4Cu_5X_9$ phase

$A_4Cu_5X_9$ compound is also a class of complex Cu-based compounds in Fig. 4(a). The crystal structure with the space group of Pc (No. 7) owns three types of Cu^+ site, a tetragonal site, a trigonal site, and a 2-fold coordination site, which forms 0D isolated $[Cu_5X_9]^{4-}$ anion, isolated by A^+ ions. Their phase stability regions versus the chemical potential of Cu and X element are shown in Fig. 4(b). Only two compounds, $Rb_4Cu_5Cl_9$ and $Cs_4Cu_5Cl_9$ own slim stability region with cyan polygon, surrounded by competing phases. The decomposition energies are 21 and 8 meV/atom for $Rb_4Cu_5Cl_9$ and $Cs_4Cu_5Cl_9$, respectively, in Table 2. Other 459-type CHP have negative ΔH_d with the ODP. It is observed that the ODP for $Rb_4Cu_5Cl_9$ phase is a disproportionation reaction, i.e., $Rb_4Cu_5Cl_9 \rightarrow 12/5Cu + 1/5Rb_2CuCl_3 + 6/5Rb_3Cu_2Cl_7$, while for the $Cs_4Cu_5Cl_9$, it is a non-redox reaction, i.e., $Cs_4Cu_5Cl_9 \rightarrow 3/4Cs_3Cu_2Cl_5 + 7/4CsCu_2Cl_3$. Experimentally, $Rb_4Cu_5Cl_9$ perovskite had been able to synthesize successfully, matches well with our predictions[15].

3.5. A_2CuX_4 compounds

Since all the above CHPs own monovalent Cu^+ ion on B

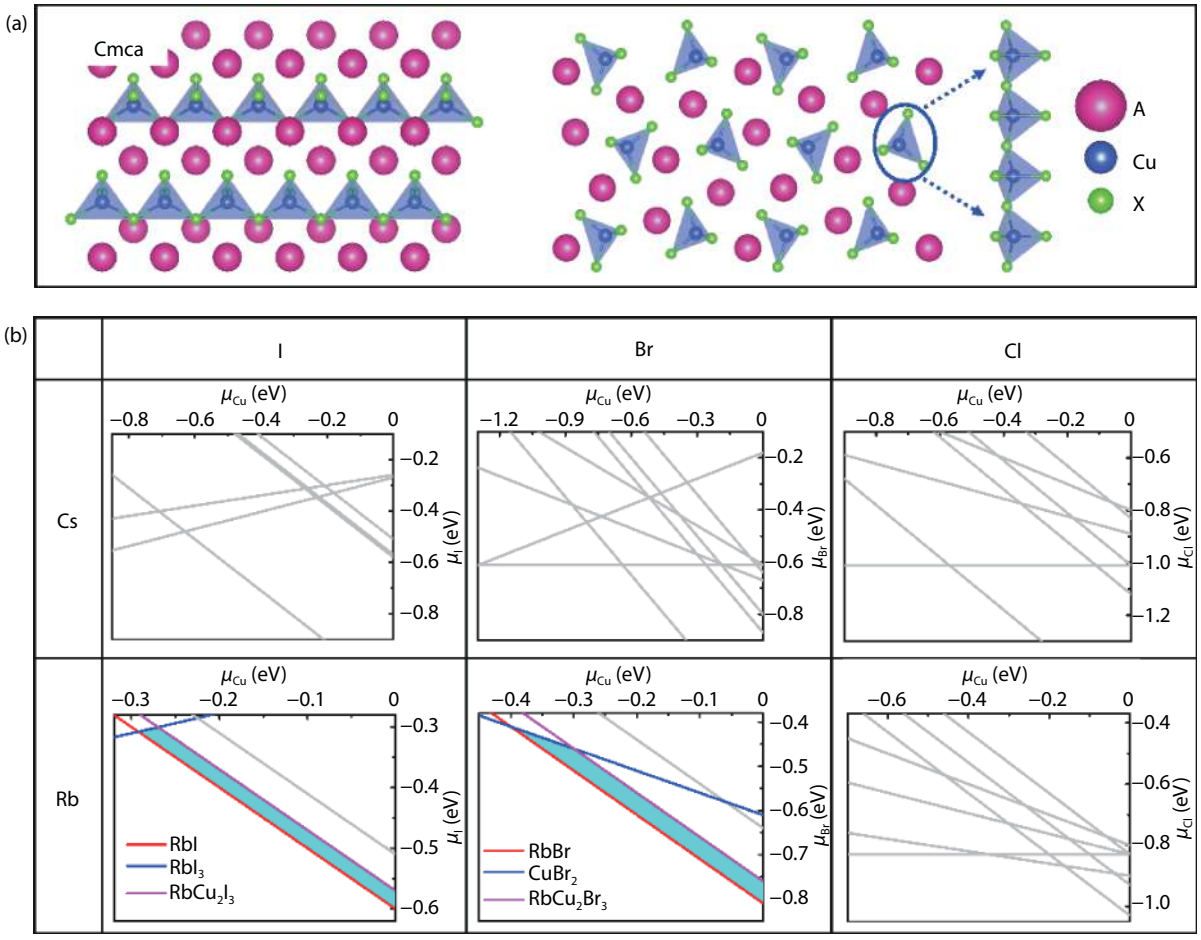

Fig. 3. (Color online) (a) The structure model of CHPs with 213-type, they possess isostructural model with Pnma symmetry, which is composed of 1D [Cu–X] tetrahedron chain with isolated alkali metal cation (Rb^+ , Cs^+). (b) Calculated phase stability regions in cyan polygon of A_2CuX_3 (A = Cs and Rb; X = I, Br, and Cl) CHPs versus μ_{Cu} and μ_X (deviation of actual chemical potential of Cu and X from that of their elementary substance). The cyan polygon region indicates thermodynamic phase stability growth interval, which is encompassed by competing phases with colored line (red, blue, and pink). A, Cu, and X atoms are in purple, coral and brown, respectively.

site, their maximum coordination number is four, induced by higher $3d^{10}$ energy level and smaller ion radius of Cu, in consistent with the report by Xiao *et al.*[16]. The CHPs with divalent Cu^{2+} ion on B site also possess abundant phases, such as 214-, 113-, and 327-type, most of which are constituted with elongated [Cu–X] octahedra, induced by Jahn-Teller distortion, except for 214-type with space group of Pnma (No. 62), which is composed of 0D [Cu–X] tetrahedra, isolated by A^+ ions, as shown in Fig. 5(a). In addition to Pnma crystal structure, Rb_2CuCl_4 compounds can exist in Cmca (No. 64) structure with 2D layers of corner-sharing $[CuCl_4]^{2-}$ octahedra[17–19]. The comparisons of total energy for non-existing compounds with two crystal structures are calculated in Table 3. The equilibrium growth region of A_2CuX_4 compounds with stable crystal phases are assessed in Fig. 5(b). Cs_2CuCl_4 undergoes non-redox ODP with ΔH_d of 34 meV/atom: $Cs_2CuCl_4 \rightarrow CsCl + CsCuCl_3$, while Cs_2CuBr_4 goes through a redox ODP with ΔH_d of 14 meV/atom, i.e., $Cs_2CuBr_4 \rightarrow 1/2CsBr + 1/4CsBr_3 + 1/2CsCuBr_3 + 1/4Cs_3Cu_2Br_5$, due to more competing phases. Experimentally, the Cu^{2+} ions of Cs_2CuBr_4 perovskite can be partially reduced to Cu^+ ions. Our calculations reveal that the Cu^+ may exist in the occurrence of $Cs_3Cu_2Br_5$ compound[17]. Although Rb_2CuCl_4 has been reported in experiments, we haven't found its stability region and its ΔH_d is also negative (–9 meV/atom) with ODP, $Rb_2CuCl_4 \rightarrow 1/2RbCl + 1/2Rb_3Cu_2Cl_7$. The discrepancies may be ascribed to the computational errors. Meanwhile, we suggested to double check the experimental results for Rb_2CuCl_4, in particular to possible existence of secondary phases including RbCl and $Rb_3Cu_2Cl_7$. For A_2CuX_4 compounds, we discover a novel and stable 214-type CHPs Rb_2CuBr_4 via phase stability region in cyan polygon and decomposition energy with ODP by ΔH_d of 10 meV/atom, i.e. $Rb_2CuBr_4 \rightarrow 2RbBr + CuBr_2$.

3.6. $ACuX_3$ compounds

Due to the divalent Cu^{2+} ions, the crystal structure of $ACuX_3$ compounds also own elongated [Cu–X] octahedra via corner- and face-sharing connection, forming spatially isolated 1D coplanar chain and 3D network through vertex-sharing, surrounded by A^+ ion in Fig. 6(a). Experimentally, $CsCuBr_3$, $CsCuCl_3$, and $RbCuCl_3$ compounds have been synthesized successfully, where $CsCuBr_3$ phase with space group of C2221 symmetry (No. 20) owns 3D network via vertex-sharing connection by coplanar double $[CuX_6]$ octahedron unit, while $CsCuCl_3$ and $RbCuCl_3$ phases possess 1D chain through face-sharing $[CuX_6]$ octahedron, they have different space group $P6_122$ (No. 178) and Pbcn (No. 60), respectively[20, 21]. The stable structures of other non-existing 113-type com-

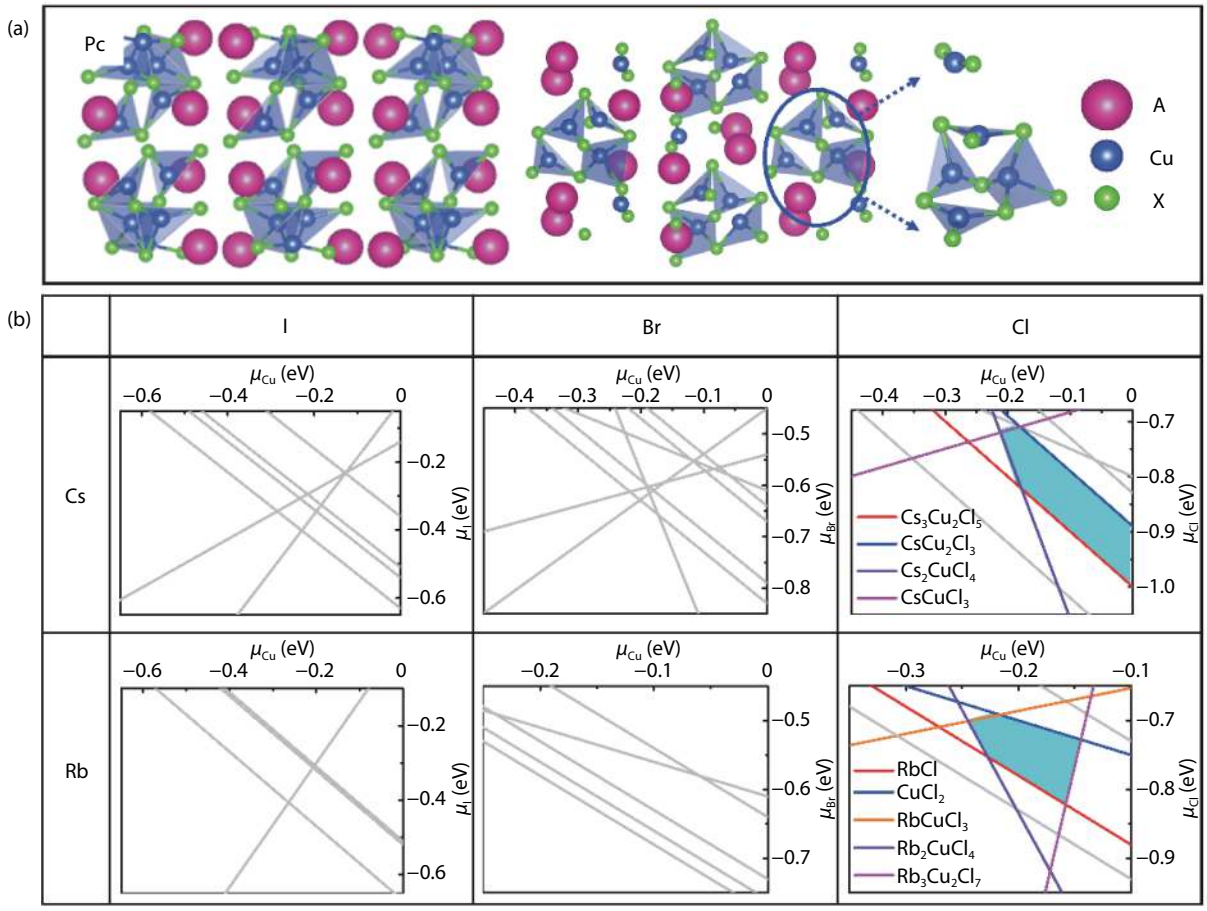

Fig. 4. (Color online) (a) The structure model of 459-type CHPs with space group of Pc, they own isolated $[Cu_5X_9]^{4-}$ anion with three types of Cu^+ ions, a tetrahedral site, a trigonal site and a 2-fold coordination site. (b) Calculated thermodynamic stability regions of 459-type CHPs against μ_{Cu} and μ_X (deviation of actual chemical potential of Cu and X from that of their elementary substance). The cyan polygon region reveals thermodynamic stable growth interval and each colored line corresponds to one most probable competing phase. A, Cu, and X atoms are in purple, coral and brown, respectively.

pounds in experiment are calculated according to the above existing crystal structures, as summed in Table 4. These stable structures with the lowest energy all own C2221 symmetry, same as $CsCuBr_3$ phase. Then the phase stability regions of the above six 113-type CHP are evaluated via thermodynamic equilibrium growth conditions, as shown in Fig. 6(b). In consistent with the experiment, $CsCuBr(Cl)_3$ compounds all possess slim stability region. Theoretical calculations did not find stability region for experiment existing $RbCuCl_3$, which may due to the computational errors or experimental ignorance of secondary phases, similar to the case of Rb_2CuCl_4. Meanwhile, we discover a new stable $RbCuBr_3$, with long and narrow stability region and positive decomposition energies of 20 meV/atom, i.e., $RbCuBr_3 \rightarrow RbBr + CuBr_2$, as shown in Table 2. This means that $RbCuBr_3$ compound is not prone to disintegrating their competing phases RbBr and $CuBr_2$. Based on the above research, we also find a new 113-type CHPs with C2221 symmetry $RbCuBr_3$ to be stable.

3.7. $A_3Cu_2X_7$ phase

Last but not least, $A_3Cu_2X_7$ phase with Cu^{2+} ion on B site owns spatially isolated 2D $[Cu_2Cl_7]^{3-}$ anion layer with double [Cu–X] octahedron layer by A^+ ions, disparity with Rb_2CuCl_4 by single [Cu–Cl] octahedron layer, as illustrated in Fig. 7(a). Their stability growth regions in cyan polygon are also assessed against μ_{Cu} and μ_X in Fig. 7(b). Except for $Cs(Rb)_3Cu_2I_7$ compounds, others possess stability region with cyan polygon, consistent with the predictions of decomposition energy in Table 2. Experimentally, $Rb_3Cu_2Cl_7$ compound has been synthesized successfully, our prediction signifies the experimental discovery[15]. In the 327-type CHP, we additionally discover three stable compounds, named as $Cs_3Cu_2Br(Cl)_7$ and $Rb_3Cu_2Br_7$. Their ODPs are all non-redox reaction, where $Cs_3Cu_2Br(Cl)_7$ compounds own similar ODP with ΔH_d of 9 and 9 meV/Å for the X site of Br and Cl element, respectively, i.e. $Cs_3Cu_2X_7 \rightarrow Cs_2CuX_4 + CsCuX_3$, X = Br, Cl. For $Rb_3Cu_2Br_7$ phase, the ODP with ΔH_d of 23 meV/Å is $Rb_3Cu_2Br_7 \rightarrow 3RbBr + 2CuBr_2$. Therefore, three new compounds in the 327-type CHPs, namely $Cs_3Cu_2Br(Cl)_7$ and $Rb_3Cu_2Br_7$ are predicted to be stable.

Table 5 summarizes the phase stability cases encompassing phase stability region and decomposition energy of ODP, whether or not they exist at room temperature. Most of existing phases are stable according to our predictions, except for Rb_2CuCl_4 and $RbCuCl_3$ perovskites because they have more binary and ternary secondary phases and computational errors. Surprisingly, we also discover 10 novel CHPs with specific stability region and positive decomposition energy with ODP (i.e., $Rb_3Cu_2I(Br)_5$, $RbCu_2Cl_3$, Rb_2CuI_3, Rb_2CuBr_4, $RbCuBr_3$, $Rb_3Cu_2Br_7$, $Cs_3Cu_2Br(Cl)_7$ and $Cs_4Cu_5Cl_9$) which have not yet

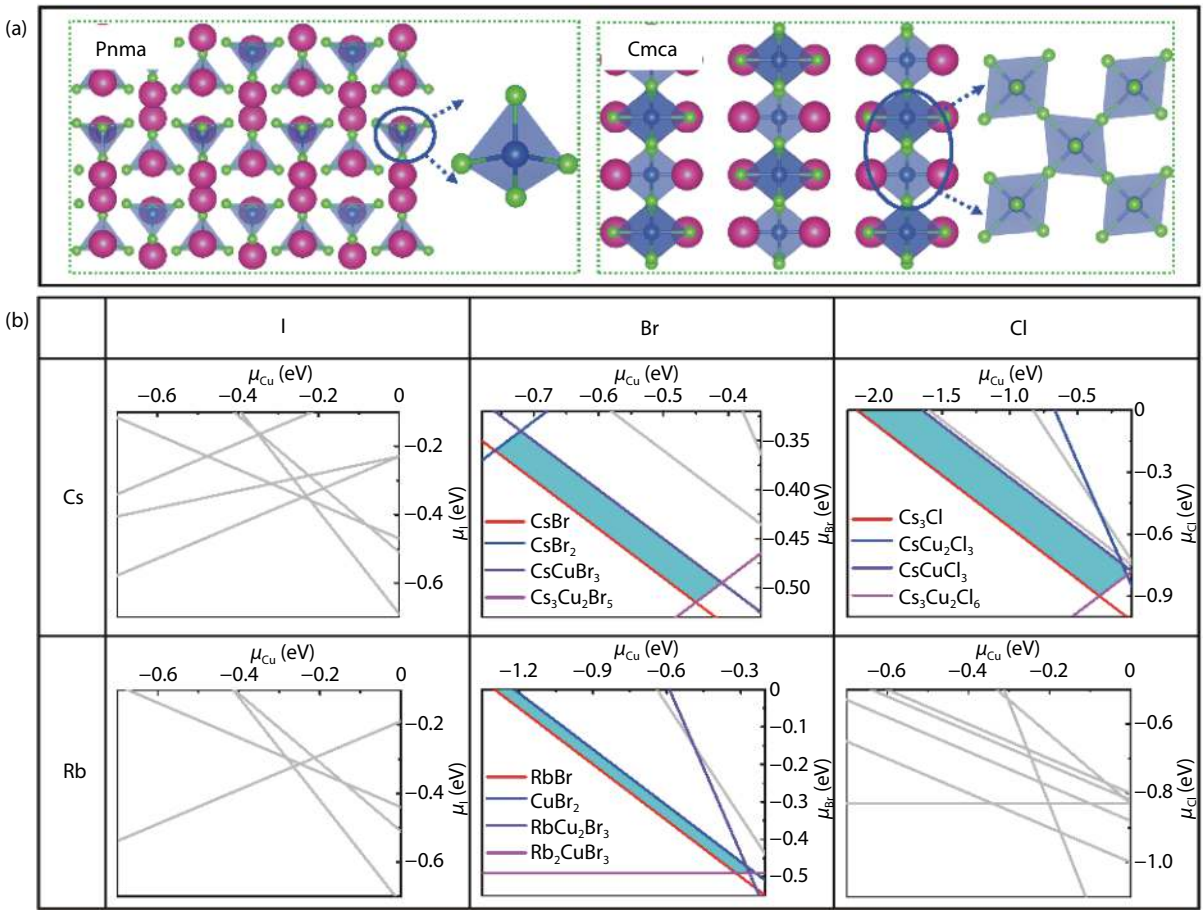

Fig. 5. (Color online) (a) The structure model of 214-type CHPs, most of them possess octahedral space group Pnma with isolated [Cu–X] tetrahedron. But for Rb_2CuCl_4, it owns Cmca symmetry with 2D $[Cu_2Cl_4]^{2-}$ layers, induced by [Cu-Cl] octahedron Jahn-Teller distortion. (b) Calculated thermodynamic stability regions of A_2CuX_4 (A = Rb and Cs; X = Cl, Br, and I) halide perovskites versus μ_{Cu} and μ_X (deviation of actual chemical potential of Cu and X from that of their elementary substance). The horizontal and vertical axis is from I to Cl element and from Cs to Rb element, respectively. The cyan polygon region shows thermodynamic stability growth interval, which is encircled by most probable competing phases with colored lines (red, blue, violet, and pink). A, Cu, and X atoms are in purple, coral and brown, respectively.

Table 3. The relative energy per formula unit (eV/f.u.) of 214-type CHPs including Cs_2CuI_4, Rb_2CuI_4, and Rb_2CuBr_4 in the different space group encompassing Pnma and Cmca, which are all non-existing phase in the ICSD.

Space group	Cs_2CuI_4	Rb_2CuI_4	Rb_2CuBr_4
Pnma	0.00	0.00	0.00
Cmca	0.29	0.33	0.04

Table 4. The relative energy per formula unit (eV/f.u.) of 113-type CHP including $CsCuI_3$, $RbCuI_3$, and $RbCuBr_3$ in the different space group containing C2221, $P6_122$, Pbcn, which are non-existing phase in the ICSD.

Space group	$CsCuI_3$	$RbCuI_3$	$RbCuBr_3$
C2221	0.00	0.00	0.00
$P6_122$	0.03	0.02	0.10
Pbcn	0.15	0.09	0.11

been reported in experiment. Our results offer importance guidance to synthesize these phases, consequently broadening the range of existing CHPs.

4. Conclusion

In summary, we have systematically studied the stability of all ternary CHPs considering thermodynamic equilibrium growth conditions and decomposition energies. They all own lower electronic dimensionality including 2D layered, 1D chained and 0D isolated unit, surrounded by A^+ ions. The coordination number of monovalent Cu (Cu^+) in the CHP is less than 4, namely, 2-fold, trigonal, tetragonal site. The vast majority of CHPs with Cu^{2+} ion possess elongated octahedron induced by Jahn-Teller distortion. Most of existing CHPs are predicted to be stable, which is in consistent with the experiment. Furthermore, we discovered ten novel phases with specific stability region and positive decomposition energy with ODP via element exchange method, i.e. $Rb_3Cu_2I(Br)_5$, $RbCu_2Cl_3$, Rb_2CuI_3, Rb_2CuBr_4, $RbCuBr_3$, $Rb_3Cu_2Br_7$, $Cs_3Cu_2Br(Cl)_7$ and $Cs_4Cu_5Cl_9$, which are not yet reported in experiment. Our predictions may provide insights for experimentalists to synthesize more novel inorganic CHPs, and will therefore tremendously expand the scope of existing CHP with promising applications.

Acknowledgements

The authors acknowledge funding support from Nation-

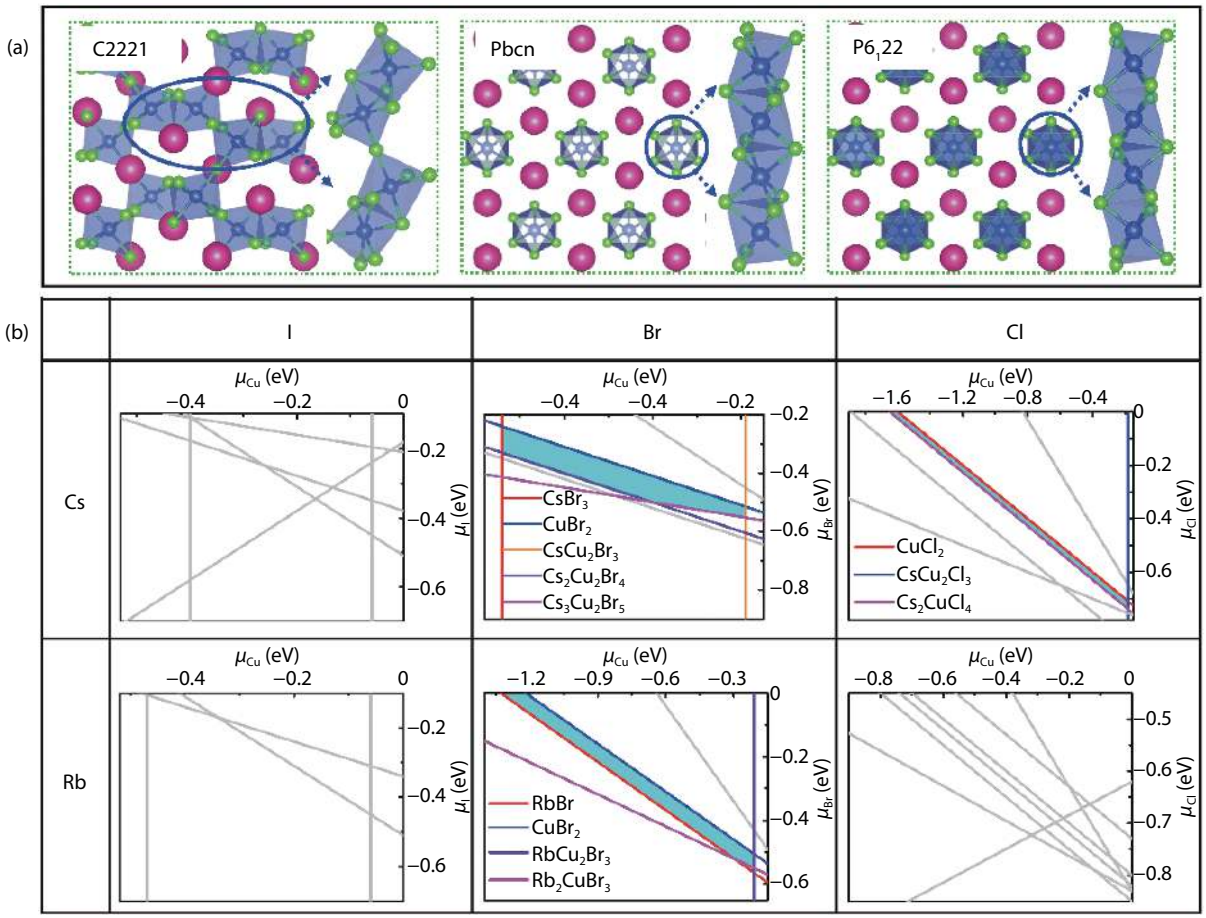

Fig. 6. (Color online) (a) The structure model of 113-type CHPs, even though they possess different structures, they all have the same [CuX_6] octahedron unit via face- and corner-sharing. (b) Calculated thermodynamic stability regions of $ACuX_3$ (A = Rb and Cs; X = Cl, Br, and I) versus μ_{Cu} and μ_X (deviation of actual chemical potential of Cu and X from that of their elementary substance). The horizontal and vertical axis is from I to Cl element and from Cs to Rb element, respectively. The cyan polygon region represents thermodynamic stable growth interval, which is surrounded by most probable competing phases using colored line (red, blue, orange, violet, and pink). A, Cu, and X atoms are in purple, coral and brown, respectively.

Table 5. Summary for the stability region and decomposition energy of ODP in the different type CHPs $A_lB_mX_n$ (A = Rb and Cs; B = Cu; X = Cl, Br, and I; *l*, *m*, and *n* are integers; named as lmn-type). For each type CHP, number 1 and 2 represent decomposition energy and stability region, respectively. '√' and '×' symbols indicate 'stable' and 'non-stable' phase, respectively. Yellow square shows that this type is existing phase from inorganic Crystal Structure Database (ICSD).

A	B	X	325		123		213		459		214		113		327	
Cs	Cu	I	√	√	√	√	×	×	×	×	×	×	×	×	×	×
		Br	√	√	√	√	×	×	×	×	√	√	√	√	√	√
		Cl	√	√	√	√	×	×	√	√	√	√	√	√	√	√
Rb		I	√	√	√	√	√	√	×	×	×	×	×	×	×	×
		Br	√	√	√	√	√	√	×	×	√	√	√	√	√	√
		Cl	×	×	√	√	√	×	√	√	×	×	×	×	√	√

Note: 1: Decomposition energy. 2: Stability region. √: Stable. × : Non-stable. : Exist.

al Natural Science Foundation of China (grant No. 11674237 and 51602211); National Key Research and Development Program of China (grant No. 2016YFB0700700); Natural Science Foundation of Jiangsu Province of China (grant No. BK20160299); the Priority Academic Program Development of Jiangsu Higher Education Institutions (PAPD); and China Post-doctoral Foundation (grant No. 7131705619). The theoretical work was carried out at National Supercomputer Center in Tianjin and the calculations were performed on TianHe-1(A).

References

[1] Sun Y, Giebink N C, Kanno H, et al. Management of singlet and triplet excitons for efficient white organic light-emitting devices. Nature, 2006, 440(7086), 908

[2] Luo J, Wang X, Li S, et al. Efficient and stable emission of warm-white light from lead-free halide double perovskites. Nature, 2018, 563(7732), 541

[3] Tan Z K, Moghaddam R S, Lai M L, et al. Bright light-emitting diodes based on organometal halide perovskite. Nat Nanotechnol, 2014, 9(9), 687

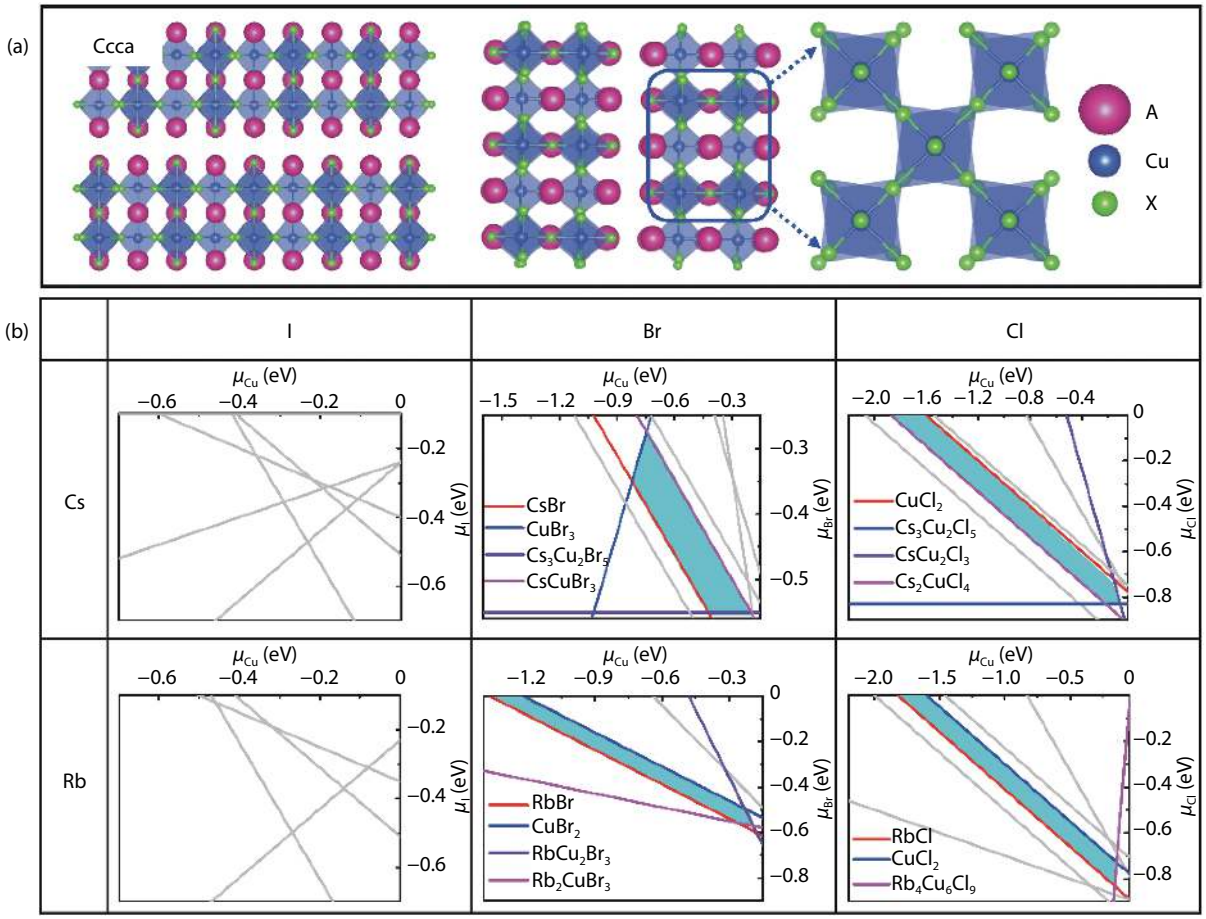

Fig. 7. (Color online) (a) The structure model of 327-type CHPs, they all own tetragonal space group Ccca with isolated $[Cu_2X_7]^{3-}$ anion composing of elongated [Cu–X] octahedron unit. (b) Calculated thermodynamic stability regions of 327-type CHPs versus μ_{Cu} and μ_X (deviation of actual chemical potential of Cu and X from that of their elementary substance). The cyan polygon region represents phase stability growth condition, which is encircled by competing phases using colored line (red, blue, violet, and pink). A, Cu, and X atoms are in purple, coral and brown, respectively.

[4] Yin W J, Shi T, Yan Y. Unique properties of halide perovskites as possible origins of the superior solar cell performance. Adv Mater, 2014, 26(27), 4653

[5] Cho H, Jeong S H, Park M H, et al. Overcoming the electroluminescence efficiency limitations of perovskite light-emitting diodes. Science, 2015, 350(6265), 1222

[6] Li J, Bade S G R, Shan X, et al. Single-layer light-emitting diodes using organometal halide perovskite/poly(ethylene oxide) composite thin films. Adv Mater, 2015, 27(35), 5196

[7] Saidaminov M I, Almutlaq J, Sarmah S, et al. Pure Cs_4PbBr_6: highly luminescent zero-dimensional perovskite solids. ACS Energy Lett, 2016, 1(4), 840

[8] Cha J H, Han J H, Yin W, et al. Photoresponse of $CsPbBr_3$ and Cs_4PbBr_6 perovskite single crystals. J Phys Chem Lett, 2017, 8(3), 565

[9] De Bastiani M, Dursun I, Zhang Y, et al. Inside perovskites: quantum luminescence from bulk Cs_4PbBr_6 single crystals. Chem Mater, 2017, 29(17), 7108

[10] Cortecchia D, Dewi H A, Yin J, et al. Lead-free $MA_2CuCl_xBr_{4-x}$ hybrid perovskites. Inorg Chem, 2016, 55(3), 1044

[11] Yang H, Zhang Y, Pan J, et al. Room-temperature engineering of all-inorganic perovskite nanocrsytals with different dimensionalities. Chem Mater, 2017, 29(21), 8978

[12] Yang J, Zhang P, Wei S H. Band structure engineering of $Cs_2AgBiBr_6$ perovskite through order–disordered transition: a first-principle study. J Phys Chem Lett, 2017, 9(1), 31

[13] Elseman A M, Shalan A E, Sajid S, et al. Copper-substituted lead perovskite materials constructed with different halides for working $(CH_3NH_3)_2CuX_4$-based perovskite solar cells from experimental and theoretical view. ACS Appl Mater Interfaces, 2018, 10(14), 11699

[14] Jun T, Sim K, Iimura S, et al. Lead-free highly efficient blue-emitting $Cs_3Cu_2I_5$ with 0D electronic structure. Adv Mater, 2018, 30(43), 1804547

[15] Hull S, Berastegui P. Crystal structures and ionic conductivities of ternary derivatives of the silver and copper monohalides — II: ordered phases within the $(AgX)_x$–$(MX)_{1-x}$ and $(CuX)_x$–$(MX)_{1-x}$ (M = K, Rb and Cs; X = Cl, Br and I) systems. J Solid State Chem, 2004, 177(9), 3156

[16] Xiao Z, Du K, Meng W, et al. Chemical origin of the stability difference between copper(I)- and silver(I)-based halide double perovskites. Angew Chem Int Ed, 2017, 129, 12275

[17] Yang P, Liu G, Liu B, et al. All-inorganic Cs_2CuX_4 (X = Cl, Br, and Br/I) perovskite quantum dots with blue-green luminescence. Chem Commun, 2018, 54(82), 11638

[18] Helmholz L, Kruh R F. The crystal structure of cesium chlorocuprate, Cs_2CuCl_4, and the spectrum of the chlorocuprate ion. J Am Chem Soc, 1952, 74(5), 1176

[19] Aguado F, Rodríguez F, Valiente R, et al. Three-dimensional magnetic ordering in the Rb_2CuCl_4 layer perovskite—structural correlations. J Phys Condens Matter, 2004, 16(12), 1927

[20] Lim A R, Kim S H. Study of the structural phase transitions in $RbCuCl_3$ and $CsCuCl_3$ single crystals with the electric-magnetic-type interactions using a ^{87}Rb and ^{133}Cs nuclear magnetic resonance spectrometer. J Appl Phys, 2007, 101, 083519

[21] Kousaka Y, Koyama T, Miyagawa M, et al. Crystal growth of chiral magnetic material in $CsCuCl_3$. J Phys Conf Ser, 2014, 502, 012019

[22] Kresse G, Furthmüller J. Efficient iterative schemes for ab initio total-energy calculations using a plane-wave basis set. Phys Rev B, 1996, 54, 11169

[23] Blöchl P E. Projector augmented-wave method. Phys Rev B, 1994, 50, 17953

[24] Perdew J P, Burke K, Ernzerh of M. Generalized gradient approximation made simple. Phys Rev Lett, 1996, 77, 3865

[25] Persson C, Zhao Y J, Lany S, et al. n-type doping of $CuInSe_2$ and $CuGaSe_2$. Phys Rev B, 2005, 72(3), 035211

[26] Zhao X G, Yang D, Sun Y, et al. Cu–In halide perovskite solar absorbers. J Am Chem Soc, 2017, 139(19), 6718